WILEY-VCH

RESEARCH ARTICLE

HfN nanoparticles: an Unexplored Catalyst for the Electrocatalytic Oxygen Evolution Reaction

Chiara Defilippi[a], Dipak V. Shinde[b], Zhiya Dang[b], Liberato Manna[b], Christopher Hardacre[c], Adam J. Greer[c], Carmine D'Agostino[c] and Cristina Giordano[a]*

Abstract: Water electrolysis is one of the most promising methods to produce H_2 and O_2 as high potential fuels. Comparing the two half-reactions, the Oxygen Evolution Reaction (OER) is the more difficult to be optimized and still relies on expensive noble-metal based catalysts such as Ru or Ir. In this paper, we prepared nanoparticles of HfN and Hf_2ON_2 and tested them for the OER for the first time. The HfN sample, in particular, showed the highest activity, requiring an overpotential of only 358 mV at 10 mA/cm^2 in Fe-free electrolyte and, above all, exhibiting long-term stability. This result places this system amongst one of the most promising catalysts for OER tested to date, in term of sustainability, activity and stability. The prepared nanoparticles are small (less than 15 nm in diameter), well-defined in shape and crystalline, and were characterised before and after electrochemical testing also via electron microscopy (EM), Powder X-rays diffraction (PXRD) and X-rays photoelectron-spectroscopy (XPS).

Introduction

Energy production is fundamental to modern society, which relies on it to survive and develop. Current energy production almost entirely relies on burning fossil fuels, which are no longer a sustainable solution. Among reliable alternatives, the production of high potential combustibles (such as H_2) via electrolysis of water (Scheme 1) is one of the most promising methods.

$2H^+_{(aq)} + 2e^- \rightarrow H_{2(g)}$ at the cathode, E^0=0 V,
HER (Hydrogen Evolution Reaction)

$H_2O_{(l)} \rightarrow ½\ O_{2(g)} + 2H^+_{(aq)} + 2e^-$ at the anode, E^0=1.23 V,
OER (Oxygen Evolution Reaction)

ΔG_H = 273.1 KJ/mol (1.23 V) in standard condition

Scheme 1. The two half-reactions for the water-splitting: H_2 is produced at the cathode (HER) and O_2 at the anode (OER)[1].To ensure an efficient conversion, the process of water splitting requires the use of suitable catalysts, which are, to date, mainly based on noble metals (Pt for HER and IrO_x or RuO_x for OER[1,2]), because they offer a lower overpotential (η) compared to other materials and fast kinetics for driving the reaction. While Pt shows ideal activity for HER (close to zero overpotential in acidic conditions), there are no other catalysts that can catalyze OER at such low overpotentials. For example, even the most commonly employed RuO_x and IrO_x catalysts perform at overpotentials of a few hundred millivolts[3]. In this respect, OER is more difficult to be optimized compared with HER and despite extensive research, the overpotentials required to sustainably drive the OER are still very high. This has wide reaching implications considering that OER finds broader applications, e.g. in fuel cells and batteries[4]. One fundamental step to be considered for a sustainable and large-scale production of hydrogen from water splitting, besides optimising catalytic activity, is to explore readily available and cost-effective catalysts. Stability is also a key prerequisite and the ideal catalyst must be resistant under the reaction conditions, i.e. it should not undergo passivation or deactivation, and must possess high surface area, conductivity and homogeneity, to ensure an efficient electron transport.

With this aim, several classes of materials based on non-noble metals have been explored, including their alloys (e.g. Ni-Mo)[5,6], oxides and chalcogenides[1,7], and in very few cases metal carbides (MC) and nitrides (MN) [1,7–9]. Among these compounds, MN possesses the highest electronic conductivity and stability under harsh conditions[1]. MN, as well as MC, are part of the family of metallic ceramics and possess high thermal and chemical resistance, good mechanical properties and high melting point, alongside metallic behaviour (e.g. good electronic conductivity) and obviously catalytic activity. The catalytic activity of some metallic ceramics is similar to that of some noble metals[10] and some of them were found to be active not only for HER (e.g. Mo_2C[11], Mo_2N[12] and Co_xN[13]) or OER (e.g. Ni_xN and Fe_xN[13–15], Co_xN[1] and Mn_3N_2[16]), but also for the reverse electrochemical processes such as oxygen reduction reaction (ORR), the cathode reaction in the fuel cells[17–19]). In some cases, however, the material is unstable or the syntheses requires toxic ammonia flow, hindering the production on a large scale. Among metal nitrides, Hf-based nitrides are one of the less explored in catalysis and electrocatalysis. So far, only HfON has been tested with promising results towards ORR[19,20] and HER[21], but not in OER. To the best of our knowledge, no studies on hafnium nitride (HfN) have been reported. This is surprising considering that HfN is also a metallic ceramic with high melting point (>3300°C) and low electrical resistivity (27 μΩ*cm)[22]. Furthermore, it is expected to have chemical and physical properties similar to Zr-based materials, which was recently addressed as a high performing electro-catalyst from theoretical studies[23]. In addition, Hf is readily available and more abundant than Ru and Ir. For example, the price of Hf in 2010 was $563 per kilogram[20], while Ru was 8500$ per kilogram and Ir is 47500$ per kilogram[24]. One of the

[a]School of Biological and Chemical Sciences, Chemistry Department, Queen Mary University of London, Mile End Road, London E1 4NS, United Kingdom

[b]Nanochemistry Department, Istituto Italiano di Tecnologia, via Morego 30,16163 Genova, Italy

[c] School of Chemical Engineering and Analytical Science, The University of Manchester, The Mill, Sackville Street, Manchester M13 9PL, United Kingdom

*c.giordano@qmul.ac.uk

Supporting information for this article is given via a link at the end of the document

reasons behind the lack of studies for HfN might be related to the synthetic challenge related to its nanoparticles preparation. In fact, only works on HfN films (using CVD and ALD) are known[25] and no reports have been published on the formation of nanoparticles or nanofibers. Although useful for film preparation, neither ALD nor CVD allows large-scale productions. In this contribution, we present a sustainable synthesis of both HfN and Hf_2ON_2 nanoparticles and related application for the OER. The sol-gel based procedure used (known as Urea-Glass-Route, UGR)[26,27] allows the easy preparation of both the metal oxynitride (Hf_2ON_2) and the pure nitride phase (HfN) in form of well-defined and small particles (15 and 10 nm for Hf_2ON_2 and HfN, respectively), with relatively high surface area (>40 m^2/g). The change in composition is accompanied by a reduction of particles size, while reaction conditions (such as temperature and metal/urea molar ratio, R) have a significant effect on the morphology of the final material. Electrochemical tests have shown significantly improved performance using HfN over Hf_2ON_2 and HfO_2 with an overpotential of 391 mV at 10 mA/cm^2 and a Tafel slope of 94 mV/dec in Fe-free 1M NaOH electrolyte. Long-term chronopotentiometry tests (up to 24h) evidence good stability of the catalyst. These results place HfN amongst the best OER noble metal-free and iron contamination-free electro-catalysts tested so far. To the best of our knowledge, this is the first time that HfN and Hf_2ON_2 were prepared at the nanoscale and tested for OER.

Results and Discussion

Phase attribution on all prepared samples was ascertained by XRD analysis. Figure 1 shows the XRD patterns of samples prepared at different ratios and heat treatments. The pattern nicely matches that of expected Hf_2ON_2 for samples prepared with a urea/metal molar ratio R≤3, and HfN for samples prepared with ratios R>10. This difference in composition is also reflected by a difference in colour (as shown in the experimental part): light grey for the oxy-nitride phase and darker grey for the nitride.

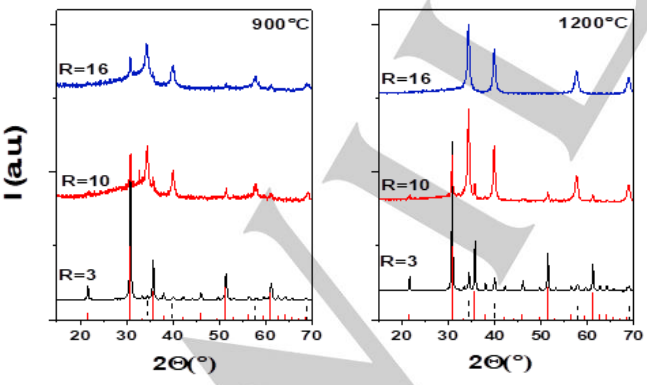

Figure 1. XRD patterns of samples prepared with different molar ratios (R=3, 10 and 16) and treated at 900°C (left) and 1200°C (right), respectively. The reference pattern of Hf_2ON_2 (ICDD: 00-050-1171, red vertical lines) and HfN (ICDD: 03-065-5056, dashed black lines) are also reported for comparison.

The possibility to address the synthesis to metal nitride over the metal oxynitride phase by changing R and/or reaction temperature is a peculiarity of the UGR and was also observed for other systems[28,29]. The reaction temperature not only affects the crystallinity of the final material but also the purity. For samples treated at T=900°C, traces of HfN can be observed in the Hf_2ON_2 phase, and vice versa, while a higher reaction temperature (T=1200°C) leads to pure HfN. The absence of the main graphitic peak from XRD pattern (expected around 26 degrees[30]) confirms the amorphous nature of the residual carbon observed from elemental analysis (Table 1). In all cases this was not found to be detrimental for the electrochemical performance of the active Hf-based material. The results of elemental analysis reported in table 1 also show a slight nitrogen deficiency in the HfN samples (wt %<6%), compared to the theoretical value (7.23%) while the C% could be due to the formation of amorphous carbon during the synthesis, as previously observed when using the UGR[24]. The crystallite size as obtained *via* Debye-Scherrer analysis shows smaller size for HfN nanoparticles and results are reported in Table 1.

Table 1. Experimental details of some representative samples obtained by varying R and heating at different temperatures under nitrogen flow. Values of nominal diameter, as well as Elemental Analysis (EA) data and surface area are reported.

Name	Main Phase (side product)	Nominal diameter [nm]		EA [wt %]		Surface area [m^2/g]
		by XRD[a]	by TEM[b]	N[c]	C	
Hf R=3 900°C	Hf_2ON_2	46	10-30 (55)	7.2	3.2	42
Hf R=10 900°C	HfN (Hf_2ON_2)	-	5-25	5.6	14.2	88
Hf R=16 900°C	HfN	20	5-25	5.8	21.2	45
Hf R=3 1200°C	Hf_2ON_2	69	13-42	5.7	3.8	37
Hf R=10 1200°C	HfN (Hf_2ON_2)	-	7-21	4.8	17.4	-
Hf R=16 1200°C	HfN	25	5-15	4.6	26.0	44

[a]Calculated on the main peak in XRD using Scherrer equation. [b]Histograms reported in the SI, values in bracket indicate that occasionally bigger particles were observed. [c] N% theoretical value in both Hf_2ON_2 and HfN is ~7%.

Crystal structures of HfN, Hf_2ON_2 and HfO_2 are reported in figure 2 (HfN is cubic, with unit cell parameter of 4.5120 Å, Hf_2ON_2 has unit cell parameter of 10.0634 Å[31]).

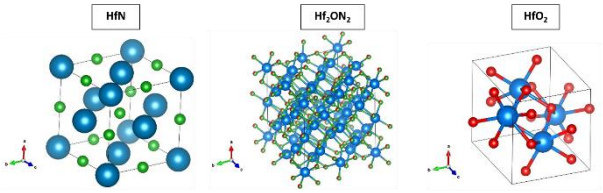

Figure 2. Crystal structures of HfN, Hf_2ON_2 and HfO_2. Cif file from ref. 36 and structures plotted using VESTA[37].

To investigate the sample's morphology, larger scale homogeneity and particle dimensions, SEM and TEM analysis were performed. SEM images of Hf_2ON_2 prepared with an initial ratio R=3 and treated at 900°C show clusters of uniform size and cube-like shape (Figure 3.A). The "edged" nature of the particles was also shown in some TEM images, where hexagonal shape nanoparticles are occasionally observed (highlighted in red in Figure 3.B). According to TEM, together with smaller nanoparticles (10-20 nm in diameter), clusters of bigger particles (50-60 nm) were also observed. TEM analysis confirmed the smaller size of the HfN nanoparticles over the Hf_2ON_2 ones (Figure 3.B-D and Figure SI.1) while SEM images of the same sample (Figure 3.C), display a needle-like shape, where nanoparticles seem to growth alongside a preferential orientation (2D structure).

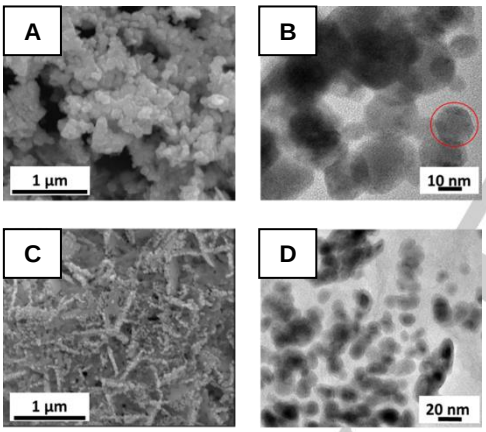

Figure 3. A) SEM and B) TEM images of sample R=3 at 900°C. C) SEM and D) TEM images of sample R=10 treated at 1200°C.

A closer examination of the TEM results performed on the same sample (Figure 3.D) evidenced the presence of small, core-shell interconnected nanoparticles. Overall, it can be concluded that the reaction conditions not only influence the final composition, but also the size and morphology of the final material. To further explore this point, additional samples were prepared with intermediate ratios, for which the TEM and SEM analysis were performed. From R=10 till R=16 the nanoparticles shape transforms from needle-like (R=10) to rod-plate like (R=12) to a layered structure for higher R (R=16) as shown in Figure 4. From this figure, it can be also observed that the 2D structure, with the preferential growth direction, is completely lost for R=16, as also confirmed by TEM (Figure 5.A). An HR-TEM study also reveals a core-shell nature of the particles synthesised at 1200°C with R=16 (Figure 5.B), where the crystalline core shows the (1-11) and (200) lattice planes for HfN (Figure 5.C) while the shell is amorphous. It must be noted that the shell is not observed for R<10 or lower reaction temperature (T<900°C).

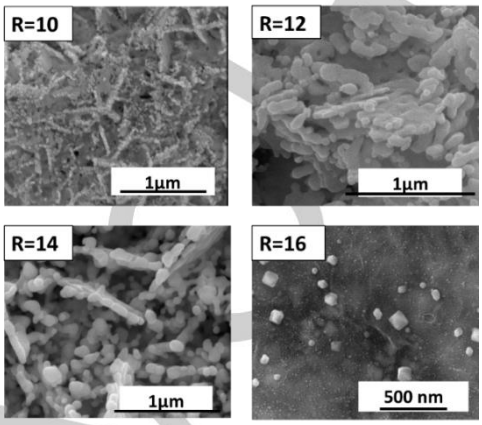

Figure 4. SEM images of HfN samples synthesised at 1200°C with different R (from 10 till 16).

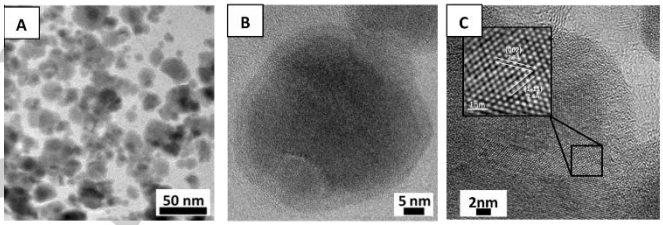

Figure 5. TEM images of HfN sample synthesised at 1200°C with R=16 at increasing magnification. A) Overview of the nanoparticles. B) Single nanoparticle showing a core-shell structure and (c) HRTEM image showing the d-spacing of the nanoparticle core.

XPS confirmed that the surface layer was oxygen-rich, which may be left after the conversion of the oxy-nitride phase in to the nitride one. The surface elemental composition (in wt.%) is reported in Table 2, while a comparison of XPS spectra bands for the Hf 4f, N 1s, C 1s and O 1s regions for each of the samples is shown in Figure 6. The fitted spectra, survey scans and peak assignment tables are shown in the supporting information (Figure SI.2-6 and Table SI.1-4).

Table 2. Elemental composition from XPS in wt.% for the samples HfO_2, HfN and Hf_2ON_2.

Element → / Compound ↓	O 1s	N 1s	Hf 4f
HfO_2	16.88	2.23	45.9
Hf_2ON_2	14.95	4.04	48.61
HfN	9.05	2.79	14.76

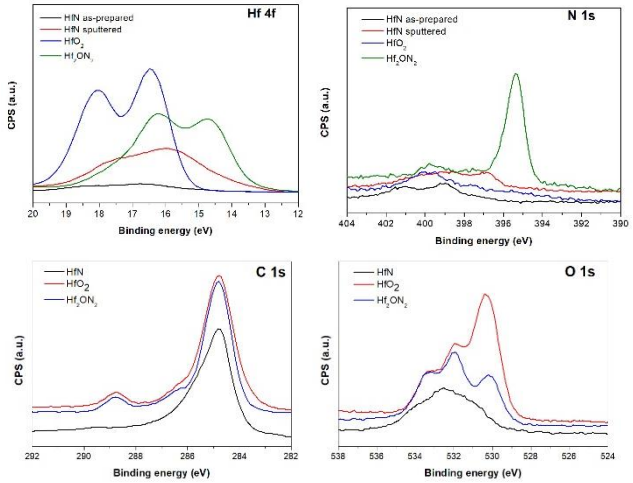

Figure 6. Comparison of XPS spectra of HfO_2, Hf_2ON_2 and HfN (before and after sputtering) in Hf 4f, N 1s, C 1s and O 1s regions.

HfO_2 was confirmed from photoelectron peaks at 16.35 and 16.88 eV (Hf 4f7/2) agreeing well with previous characterisation results[32]. Lattice oxygen was also confirmed at 530.29 eV (O 1s spectra)[32]. A more reduced Hf species was observed in the oxynitride sample, with peaks at 14.66 and 16.01 eV corresponding to Hf-N and Hf-O respectively[33,34]. The formation of the oxynitride phase was further established from the analysis of the core level N 1s spectra, where peaks in the 395-397 eV region were observed, corresponding to new Hf-N bonds[20,33,35]. The HfN sample also showed oxidized Hf $4f_{7/2}$ (16.65 eV) and N 1s at 401.34 eV, with the peak at 398.73 eV assigned to the overlap of the Hf 4p plasmon. This is consistent with the oxygen-rich outer shell of the nanoparticles, as observed by TEM on samples prepared with higher urea/metal molar ratio (R). However, following etching of the sample under argon ion bombardment, the carbonaceous species was removed, and a new peak at 396.80 eV was deconvoluted, corresponding to Hf-N [20,33,35]. The binding energy of the Hf 4f peak also shifted from 16.65 eV to 15.59 eV, further signifying the reduced Hf-N species [33,34].

Electrochemical testing. The electrocatalytic performance was examined for both Hf_2ON_2 and HfN. Commercial HfO_2 and RuO_2 were also tested to compare the OER activity. The OER activity in Fe-free electrolyte was initially tested in order to avoid iron contaminations on the working electrode, which would affect the results. This is a very important point to be considered, since it was reported that even small impurities of iron have an enormous effect on the OER activity of the catalysts[36]. In fact, a plethora of OER catalysts reported so-far are tested in non-purified electrolytes containing traces of Fe impurities but this does not allow to determine the actual catalytic activity of the material under investigation. Initially, the samples were deposited on glassy carbon electrodes to measure the intrinsic OER activities. CVs were repeated until a reproducible voltammogram was obtained. In addition, commercial RuO_2, a benchmark catalyst for OER[1], was used to compare the activity of our catalysts. The overpotential needed to achieve 10 mA/cm^2 current density was used as a parameter to compare different catalysts studied, herein. As shown in figure 8A, RuO_2 requires, as expected, lowest overpotential (321 mV) to achieve 10 mA/cm^2 catalytic current, followed by HfN (504 mV), HfO_2 (497 mV at 1 mA/cm^2) and Hf_2ON_2 (577 mV at 8 mA/cm^2). The overpotential values are in line with those observed for widely studied $Ni(OH)_2$ catalyst measured in Fe-free electrolytes[36]. The lower overpotential of HfN compared to Hf_2ON_2 and HfO_2 can be attributed to better electrical conductivity of HfN[22], which results in efficient charge transport. Tafel analysis was performed to gain insights on the mechanism underlying OER on our catalysts (figure 8B). The Tafel slope values are summarized in Table 3 which lie in the range of 130-300 mV/dec range for HfN and Hf_2ON_2 while a value of 385 mV/dec was obtained for HfO_2. Next, we proceeded to measure the OER activity of our catalysts in normal commercially available NaOH electrolyte, which contains traces of Fe impurities, as this would be the obvious electrolyte of choice for commercial alkaline electrolysers. Figure 8C reports the CVs of the catalysts measured in 1M NaOH electrolyte (non-purified). As can be seen, the OER current densities increased substantially for HfN and Hf_2ON_2, while HfO_2 showed similar activity. The Tafel plots are reported in figure 8D and the slope values reported in table 4 indicate improved OER kinetics over HfN in the normal electrolyte. This is in line with the improvement observed for previously studied $Ni(OH)_2$ catalysts[36].

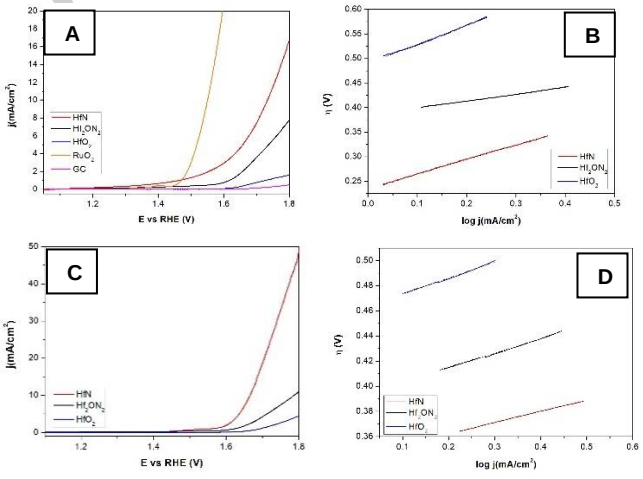

Figure 8. A) OER measurements using glassy carbon as supporting electrode, the CV of glassy carbon is reported for comparison. B) Tafel plots comparison in 1M NaOH purified electrolyte, C) OER measurements in 1M NaOH (non-purified) electrolyte and D) Tafel plots comparison in 1M NaOH normal electrolyte for HfN, is Hf_2ON_2 and RuO_2. The dashed black lines represent the linear fitting to calculate Tafel slopes.

To better understand the reason behind the good performance of HfN as compared to Hf_2ON_2, double layer capacitance (C_{dl}) measurements were performed to determine their electrochemically active surface area (ECSA), following the procedure reported in literature[37]. The CVs for this purpose were measured in the range of 0-0.1 V vs Ag/AgCl where no faradic charge transfer occurred (See figure SI. 7). Despite having nearly similar C_{dl} values (figure SI.8.), HfN showed much higher activity for OER as compared to Hf_2ON_2, indicating higher intrinsic activity of HfN towards this reaction. The Cdl values for HfO_2 were three

orders of magnitude lower than that of HfN, indicating lower ECSA of the former (see figure SI. 8). This, combined with the insulating nature of HfO_2, might be the cause for the lowest OER activity of HfO_2. This highlights that the catalyst having high conductivity with high ECSA is required to achieve high OER activity and that presence of Fe impurity only cannot guarantee the high OER activity.

This is further supported by our electrochemical impedance spectroscopy (EIS) measurements. Nyquist plots of the impedance data are reported in figure 9, both for the purified and normal electrolyte. All the catalysts studied herein exhibit a single semicircle, which is related to the charge transfer resistance (R_{ct}) associated with OER process. The size of the semicircle in the low-frequency range increases from HfN<Hf_2ON_2<HfO_2, indicating that OER is most favoured on HfN electrodes and least favoured on HfO_2 electrodes[38]. Furthermore, in normal electrolytes, the trend in R_{ct} values remains the same while the values decrease considerably in all the cases as shown in Table 4. This further highlights the efficient OER over HfN in both purified and normal electrolytes.

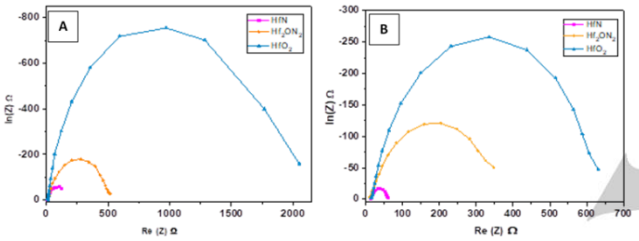

Figure 9. Nyquist plots of HfN, Hf_2ON_2 and HfO_2 at 1.72V vs RHE in A) purified 1M NaOH and B) in normal 1M NaOH.

In order to further maximize the OER catalytic activity of HfN, we deposited the catalyst ink on Ni foam, a support with uniform three-dimensional network, high surface area and good electron transport[39]. As can be seen from the polarization curves reported in Figure 10, OER currents improved significantly in both purified and normal electrolytes. The HfN-NF catalyst achieves 10 mA/cm^2 of OER current at an overpotential of only 391 mV in purified electrolyte, while in the normal electrolyte this value further improves to 358 mV. The Tafel slope values also improve in both cases indicating better kinetics of OER on HfN on porous 3D NF substrate. The overpotential values obtained here are comparable to those of the widely studied Ni and Co-based catalysts and could be further improved by increasing ECSA of the HfN catalyst[7]. A comparison of the overpotential and Tafel slope values for the tested HfN with other nitrides-based catalysts reported in literature and tested in similar conditions is reported in figure SI.6.

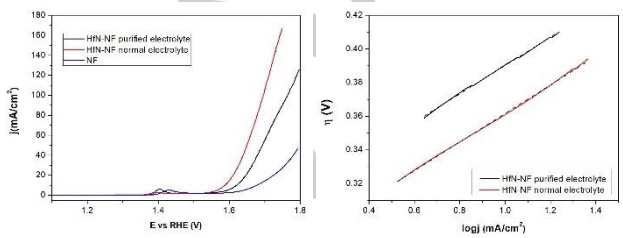

Figure 10. A) OER measurements in 1M NaOH purified and non-purified electrolyte, using nickel foam (NF) as support for HfN. The CV of Nickel foam is shown for comparison. B) Tafel plots comparison for HfN, on nickel foam (NF), measured both in the normal and in the purified electrolyte. The dashed black lines represent the linear fitting to calculate Tafel slopes.

Table 3. Over potential, Tafel slope and average Cd values for the HfN, Hf_2ON_2 and HfO_2 catalysts, tested with different supports both in the normal and in the purified electrolyte.

Catalyst	Over potential (mV) at 10 mA/cm^2	Tafel slope (mV/dec)	Average C_d (mF/cm^2)
HfN (GC) purified electrolyte	504 mV	295	0.0013
HfN (GC) normal electrolyte	436 mV	89	
Hf_2ON_2 (GC) purified electrolyte	577 mV (at 8mA/cm2)	139	0.0014
Hf_2ON_2 (GC) normal electrolyte	557 mV	115	
HfO_2 (GC) purified electrolyte	497 mV (at 1mA/cm2)	385	$3.9*10^{-5}$
HfO_2 (GC) normal electrolyte	585 mV (at 5mA/cm2)	128	
HfN (NF) purified electrolyte	391 mV	84	
HfN (NF) normal electrolyte	358 mV	85	

Table 4. Charge transfer resistance values for the HfN, Hf_2ON_2 and HfO_2 catalysts, both in the normal and in 1M NaOH purified electrolyte.

Sample	Rct (Ω)	
	Purified electrolyte	Normal electrolyte
HfN	110	47
Hf_2ON_2	505	338
HfO_2	2039	618

Finally, the stability of the HfN catalyst was measured under OER operating conditions at a constant applied current density of 10 mA/cm^2 for 24h as reported in figure 11. From this figure, it can be appreciated that the potential required to maintain the applied current density remains nearly constant through the 24h indicating excellent stability of our HfN catalyst.

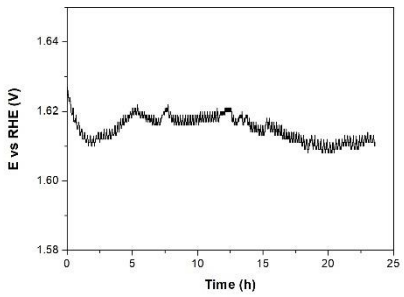

Figure 11. Chronopotentiometry measurement of HfN sample on NF, measured at 10 mA/cm^2.

The morphology (via TEM) and composition (via PXRD) of the HfN catalyst was examined after the stability tests. As shown in figure SI.9-11 and table SI.5, no significant changes were observed, further confirming the stability of our HfN catalyst.

Conclusion

Well-defined and small nanoparticles of Hf_2ON_2 and HfN were prepared and tested for the first time for OER. An extensive characterization was made before and after testing, using powder XRD, SEM, HR-TEM and XPS. The OER performance of Hf_2ON_2 and HfN were compared in Fe-free purified and normal electrolyte (1M NaOH), using both glassy carbon and nickel foam as supports, to determine the actual catalytic activity of the materials under investigation. HfN showed the best activity, attributed to its high electrical conductivity, favouring an efficient charge transport. The HfN catalyst achieved, 10 mA/cm^2 of OER current at an overpotential of only 391 mV and 358 mV in purified and normal electrolyte, respectively, with a Tafel slope of 84 and 85 mV/dec. Long-term stability for 24h of HfN under OER operating conditions at a constant current density of 10 mA/cm^2 was tested and the potential remained nearly constant indicating excellent stability of our HfN catalyst. The stability was further confirmed by PXRD and TEM done on the catalysts after OER test. The results presented so far place the system among the most promising catalyst for OER tested to date, in term of sustainability, activity and stability.

Experimental Section

Nanoparticles preparation. In a typical experiment, hafnium (IV) chloride ($HfCl_4$, VWR 98+%)/methanol solutions (1.24M) were prepared and added with suitable amounts of urea ($CO(NH_2)_2$, Sigma Aldrich 99%) to reach a final urea/$HfCl_4$ molar ratio (R) from 1 to 16. Mixtures were stirred till a clear, viscous yet transparent solution was observed (Fig.12 A). The gel-like precursor was then thermally treated under N_2 flow up to 1200˚C for 3 h and thereafter cooled to room temperature. The final product was a fine powder, light grey for samples treated up to 900°C (Fig.12 B) and dark grey for the ones treated up to 1200°C (Fig.12 C). For comparison, HfO_2 was also prepared via UGR, using a mixed flow of N_2 and air. The usefulness of the UGR to prepare metal oxides was also previously reported[40].

Figure 12. Photographs showing the precursor solution (A), the final product obtained after heat treatment under N_2 flow at 900 °C (B) and 1200°C (C), respectively. Phase attribution was made by PXRD study (see text for details).

Electrochemical measurements. The prepared HfN and Hf_2ON_2 were tested for OER using IVIUM Compactstat potentiostat and their performances compared with those of commercial HfO_2 (Sigma Aldrich, 98%) and RuO_2 (Sigma Aldrich, 99.9%). The catalyst ink was prepared grounding in a mortar 2.5 mg of the powder catalyst and then adding 100 microliters of Nafion® solution, 0.25% in ethanol (5 wt % in lower aliphatic alcohols and 15−20% water, Sigma Aldrich). For the catalysts deposited on glassy carbon substrates, conductive carbon black was added (carbon black super P Alfa-Aesar, 99+%). The ink was ultrasonicated for 30 min and then drop-cast with different loadings on different electrode support, e.g. glassy carbon (3 mm diameter) and nickel foam (Sigma Aldrich, 95%, foam, thickness 1.6 mm, bulk density 0.45g/cm^3, porosity 95%) and allowed to dry at room temperature in ambient air. The loading for each catalyst was optimized to obtain maximum OER activity. The best ink loading was found to be 5 µl for Hf_2ON_2 (1.96mg/cm^2), 10 µl for HfN (4.57mg/cm^2) and 20 µl for HfO_2 (7.8 mg/cm^2). OER measurements were conducted using a three-electrode cell set-up, using a double junction Ag/AgCl (3.8 M KCl) as a reference electrode and platinum wire as counter electrode. Cyclic voltammetry (CV) measurements were performed in 1 M NaOH electrolyte (Sigma Aldrich, >98%, diluted with Milli-Q water, 18.2 mΩ cm at 25°C) at room temperature in the range of 0-0.8 V (vs Ag/AgCl) with a scan rate of 5mV/second. Impedance measurements were performed in the frequency range from 0.1 Hz to 1 MHz. All data were iR-corrected using iR correction function of IVIUM software. The potentials were converted to RHE (reversible hydrogen electrode) scale by using the following formula: $E_{RHE}=E^0_{Ag/AgCl} + E_{Ag/AgCl} + (0.059 \times pH)$. Long-term stability measurement was conducted by chronopotentiometry at an applied current density of 10 mA/cm^2.

Electrolyte purification. Iron-free electrolyte was obtained following the procedure reported by Trotochaud et al.[36], briefly, 2 g of $Ni(NO_3)_2$*6 H_2O (Sigma Aldrich, 99.999%) were dissolved, using a centrifuge tube, in few ml of water (Milli-Q water, 18.2 mΩ cm at 25°C), followed by the addition of 20 ml of 1M NaOH. This resulted in the precipitation of green coloured $Ni(OH)_2$. The mixture underwent several cycles of centrifuging and supernatant removal, adding a fresh mixture of 20 ml water/ 1 ml 1M NaOH every time. After several washings, the tube was filled with 1M NaOH, shaken and left overnight. The purified electrolyte was then used for OER testing in Fe free conditions.

Acknowledgements

C.G. and C.D. acknowledge QMUL for financial support. All authors acknowledge Dr. M. Prato (Materials Characterization Facility – Istituto Italiano di Tecnologia) for support in XPS data acquisition and Mr Maurizio Leo from Nanoforce Technology Ltd for his kind help during materials preparation.

Keywords: hafnium nitride, hafnium oxide, hafnium oxynitride, nanoparticles, nitrides, oxygen evolution reaction (OER), Urea Glass Route.

[1] N.-T. Suen, S.-F. Hung, Q. Quan, N. Zhang, Y.-J. Xu, H. M. Chen, *Chemical Society Reviews* **2017**, *46*, 337–365.
[2] Y. Zheng, Y. Jiao, M. Jaroniec, S. Z. Qiao, *Angewandte Chemie International Edition* **2015**, *54*, 52–65.
[3] Y. Lee, J. Suntivich, K. J. May, E. E. Perry, Y. Shao-Horn, *The Journal of Physical Chemistry Letters* **2012**, *3*, 399–404.
[4] D. V. Shinde, L. D. Trizio, Z. Dang, M. Prato, R. Gaspari, L. Manna, *Chemistry of Materials* **2017**, *29*, 7032–7041.
[5] M. Li, Y. Zhu, H. Wang, C. Wang, N. Pinna, X. Lu, *Advanced Energy Materials* **2019**, *9*, 1803185.
[6] M. Wang, Z. Dang, M. Prato, D. V. Shinde, L. De Trizio, L. Manna, *ACS Applied Nano Materials* **2018**, *1*, 5753–5762.
[7] M. Tahir, L. Pan, F. Idrees, X. Zhang, L. Wang, J.-J. Zou, Z. L. Wang, *Nano Energy* **2017**, *37*, 136–157.
[8] D. H. Youn, S. Han, J. Y. Kim, J. Y. Kim, H. Park, S. H. Choi, J. S. Lee, *ACS Nano* **2014**, *8*, 5164–5173.
[9] D. H. Youn, G. Bae, S. Han, J. Y. Kim, J.-W. Jang, H. Park, S. H. Choi, J. S. Lee, *Journal of Materials Chemistry A* **2013**, *1*, 8007.
[10] R. B. Levy, M. Boudart, *Science* **1973**, *181*, 547–549.
[11] L. Ma, L. R. L. Ting, V. Molinari, C. Giordano, B. S. Yeo, *J. Mater. Chem. A* **2015**, *3*, 8361–8368.
[12] U. Joshi, J. Lee, C. Giordano, S. Malkhandi, B. S. Yeo, *Physical Chemistry Chemical Physics* **2016**, *18*, 21548–21553.
[13] N. Han, P. Liu, J. Jiang, L. Ai, Z. Shao, S. Liu, *Journal of Materials Chemistry A* **2018**, *6*, 19912–19933.
[14] F. Yu, H. Zhou, Z. Zhu, J. Sun, R. He, J. Bao, S. Chen, Z. Ren, *ACS Catalysis* **2017**, *7*, 2052–2057.
[15] M. Shao, Q. Chang, J.-P. Dodelet, R. Chenitz, *Chemical Reviews* **2016**, *116*, 3594–3657.
[16] A. Leineweber, R. Niewa, H. Jacobs, W. Kockelmann, *Journal of Materials Chemistry* **2000**, *10*, 2827–2834.
[17] L. Cao, Y. Yu, S. Huang, yanpeng li, stephan N. steinmann, W. Yang, *Nano Lett.* **2014**, *14*, 2, 553-558.
[18] D. Ham, J. Lee, *Energies* **2009**, *2*, 873–899.
[19] M. Chisaka, Y. Suzuki, T. Iijima, Y. Ishihara, R. Inada, Y. Sakurai, *ECS Electrochemistry Letters* **2012**, *1*, F4–F8.
[20] M. Chisaka, H. Muramoto, *ChemElectroChem* **2014**, *1*, 863–867.
[21] X. Yang, F. Zhao, Y.-W. Yeh, R. S. Selinsky, Z. Chen, N. Yao, C. G. Tully, Y. Ju, B. E. Koel, *Nature Communications* **2019**, *10*, 1543.
[22] Y. Zhong, X. Xia, F. Shi, J. Zhan, J. Tu, H. J. Fan, *Advanced Science* **2016**, *3*, 1500286.
[23] Y. Abghoui, A. L. Garden, J. G. Howalt, T. Vegge, E. Skúlason, *ACS Catalysis* **2016**, *6*, 635–646.
[24] **2019**.
[25] S. Karwal, M. A. Verheijen, B. L. Williams, T. Faraz, W. M. M. Kessels, M. Creatore, *Journal of Materials Chemistry C* **2018**, *6*, 3917–3926.
[26] C. Giordano, C. Erpen, W. Yao, M. Antonietti, *Nano Letters* **2008**, *8*, 4659–4663.
[27] C. Giordano, C. Erpen, W. Yao, B. Milke, M. Antonietti, *Chemistry of Materials* **2009**, *21*, 5136–5144.
[28] Q. Gao, S. Wang, Y. Ma, Y. Tang, C. Giordano, M. Antonietti, *Angewandte Chemie International Edition* **2012**, *51*, 961–965.
[29] B. Milke, C. Wall, S. Metzke, G. Clavel, M. Fichtner, C. Giordano, *Journal of Nanoparticle Research* **2014**, 2895.
[30] C. Giordano, A. Kraupner, I. Fleischer, C. Henrich, G. Klingelhöfer, M. Antonietti, *Journal of Materials Chemistry* **2011**, *21*, 16963.
[31] The “Inorganic Crystal Structure Database (ICSD),” can be found under http://www2.fiz-karlsruhe.de/icsd_web.html.
[32] D. Barreca, A. Milanov, R. A. Fischer, A. Devi, E. Tondello, *Surface Science Spectra* **2007**, *14*, 34–40.
[33] M. Lee, Z.-H. Lu, W.-T. Ng, D. Landheer, X. Wu, S. Moisa, *Applied Physics Letters* **2003**, *83*, 2638–2640.
[34] Y.-H. Chou, H.-T. Chiu, T.-F. Kuo, C.-C. Chi, S.-H. Chuang, *Applied Physics Letters* **2006**, *89*, 252901.
[35] A. Arranz, C. Palacio, *Surface Science Spectra* **2004**, *11*, 33–42.
[36] M. S. Burke, M. G. Kast, L. Trotochaud, A. M. Smith, S. W. Boettcher, *Journal of the American Chemical Society* **2015**, *137*, 3638–3648.
[37] G. Li, L. Anderson, Y. Chen, M. Pan, P.-Y. Abel Chuang, *Sustainable Energy & Fuels* **2018**, *2*, 237–251.
[38] H. Ma, C. Liu, J. Liao, Y. Su, X. Xue, W. Xing, *Journal of Molecular Catalysis A: Chemical* **2006**, *247*, 7–13.
[39] C. Walter, P. W. Menezes, S. Orthmann, J. Schuch, P. Connor, B. Kaiser, M. Lerch, M. Driess, *Angewandte Chemie International Edition* **2018**, *57*, 698–702.
[40] F. Armetta, M. L. Saladino, C. Giordano, C. Defilippi, Ł. Marciniak, D. Hreniak, E. Caponetti, *Scientific Reports* **2019**, *9*, 3368.

Entry for the Table of Contents

RESEARCH ARTICLE

HfN nanoparticles prepared via UGR are highly active and stable electro-catalyst for the water splitting semi-reaction OER (Oxygen Evolution Reaction). The results presented place HfN amongst one of the most promising catalysts for OER tested to date, in term of sustainability, activity and stability.

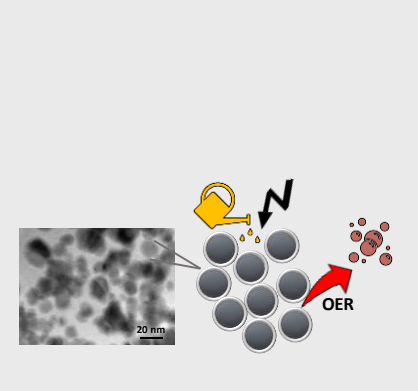

*Chiara Defilippi, Dipak V. Shinde, Zhiya Dang, Liberato Manna, Christopher Hardacre, Adam Greer, Carmine D'Agostino and Cristina Giordano**

Page No. – Page No.

Title